Development of a diffusion MR pipeline for the investigation of white matter microstructure

Master's thesis

Benjamin Powell

Supervisor:	Lajos R. Kozák, M.D, Ph.D. *assistant professor* *MR Research Centre* *Semmelweis University Budapest*
Departmental supervisor:	Dr. Dávid Légrády, Ph.D. *associate professor* *Institute of Nuclear Techniques* *Budapest University of Technology and Economics*

Budapest University of Technology and Economics
2016

Diplomamunka feladat a Fizikus mesterképzési (MSc) szak hallgatói számára

A hallgató neve:	**Powell Benjámin Márk**	szakiránya: **orvosi fizika**
A diplomamunkát gondozó (a záróvizsgát szervező) tanszék:		**Nukleáris Technika Tanszék**

A diplomamunka készítésének helye:	**Semmelweis Egyetem MRKK**	
A témavezető neve: **dr. Kozák Lajos Rudolf**		A konzulens neve: **Légrády Dávid** (külső témavezető esetén kijelölt tanszéki munkatárs)
– munkahelye: **Semmelweis Egyetem MRKK**		
– beosztása: **egyetemi adjunktus**		– beosztása: **egyetemi docens**
– e-mail címe: **lkozak@mrkk.sote.hu**		– e-mail címe: **legrady@reak.bme.hu**

A diplomamunka címe:	**Diffúziós MR adatfeldolgozó eljárás fejlesztése a fehérállományi mikrostruktúra vizsgálatára**	azonosítója: **DM-2016-43**

A téma rövid leírása, a megoldandó legfontosabb feladatok felsorolása:

A diffúzió-súlyozott vizsgálatok napjainkban a Mágneses Rezonancia Képalkotás (MRI) egyik intenzíven kutatott területe. Speciális mérési szekvencia alkalmazásával, a vízmolekulák diffúziós mozgásának mérésén keresztül, az agy fehérállományi struktúrája in vivo vizsgálatokban feltérképezhető, különböző hatások okozta változásai nyomon követhetők. A hallgató feladatai: - A Semmelweis Egyetem MR Kutató Központjában alkalmazott adatfeldolgozó eljárások megismerése. - Nyilvános adatbázisból származó, Alzheimer-kóros, enyhe kognitív deficittel rendelkező és kontrol alanyok DWI-adatainak előfeldolgozása. - Az Alzheimer-kórral összefüggő strukturális változások feltérképezése a megismert módszerek felhasználásával. - Részvétel új módszer kidolgozásában a megtalált kóros területek diffúziós profiljában jelentkező eltérések azonosítására.

A feladat kiadásának időpontja:	**2015 szeptember**

Témavezető vagy tanszéki konzulens aláírása:	A diplomamunka témakiírását jóváhagyom (tanszékvezető aláírása):

Önállósági nyilatkozat

Declaration of independent work

Alulírott Powell Benjámin a Budapesti Mőszaki és Gazdaságtudományi Egyetem Fizikus mesterszak (MSc) Orvosi fizika szakirányának hallgatója kijelentem, hogy ezt a diplomamunkát meg nem engedett segítség igénybevétele nélkül, saját magam készítettem. Minden olyan szövegrészt, adatot, diagramot, ábrát, vagy bármely más elemet, amelyet vagy szó szerint, vagy azonos értelemben, de átfogalmazva másoktól vettem át, a forrás megadásával egyértelmően megjelöltem.

Budapest, 2016. 06. 10.

…………………………

(Powell Benjámin)

Table of contents

1   Introduction

The goal of my thesis was to contribute to on-going research being conducted into the diagnosis of Alzheimer's disease with diffusion tensor imaging (DTI) at the MR Research Centre of Semmelweis University.

DTI is able to provide information about the microstructure of tissues such as the white matter of the brain. DTI is based on diffusion weighted (DW) MRI where the diffusion of water molecules can be traced in specific directions. With the relevant mathematical methods DW MRI provides a platform to gain knowledge about the spatial distribution of the local diffusion in a voxel by measuring the signal attenuation coming from each voxel during the aquisition of the DW image. Because white matter is a highly structured tissue the spatial distribution of the local diffusion can provide information about this structure inside the brain. The mathematical formalism used to describe the spatial distribution of diffusion makes use of tensors, from which scalar measures can be defined to characterize and quantify the local diffusion in each voxel. By the comparison of such parameter maps between cognitively normal and Alzheimer's disease affected subjects, structural changes in white matter can be studied during the progression of dementia.

A prerequisite of such comparisons of parameter maps are the normalisation of the image data of the subjects compared into a common anatomical coordinate system.

A pipeline was implemented for the comparison of such DTI data with a whole brain voxel-based analysis (VBA) method. Improvements were made to the standard VBA approach by including several covariates to the statistical analysis. Region-of-interest-level correlation analysis was also implemented for further validation of the results of the whole brain VBA method.

2 Diffusion tensor imaging (DTI)

Diffusion refers to the process of random motion of a particle. A measure of this random motion is the mean squared displacement of the particle which describes the spatial deviation of a particle to a reference point over time. Einstein was the first who described the relationship of the mean squared displacement for free (isotropic) diffusion [9] :

$$\langle r \rangle^2 = 2NDt \tag{2.1}$$

where N = 1,2,3 depends on the number of dimensions, D is the diffusion coefficient and t is the elapsed time. If diffusion is considered anisotropic, meaning there is some kind of structure hindering diffusion in one or more directions a scalar value is no longer sufficient in describing the process of diffusion in all directions. In the anisotropic case in 3 dimensions the diffusion coefficient is described by a 3×3 tensor. Because diffusion has to be described by real values, this means the tensor is symmetric leaving only six independent elements to the tensor:

$$\boldsymbol{D} = \begin{bmatrix} D_{xx} & D_{xy} & D_{xz} \\ D_{xy} & D_{yy} & D_{yz} \\ D_{xz} & D_{yz} & D_{zz} \end{bmatrix} \tag{2.2}$$

2.1 Diffusion in white matter
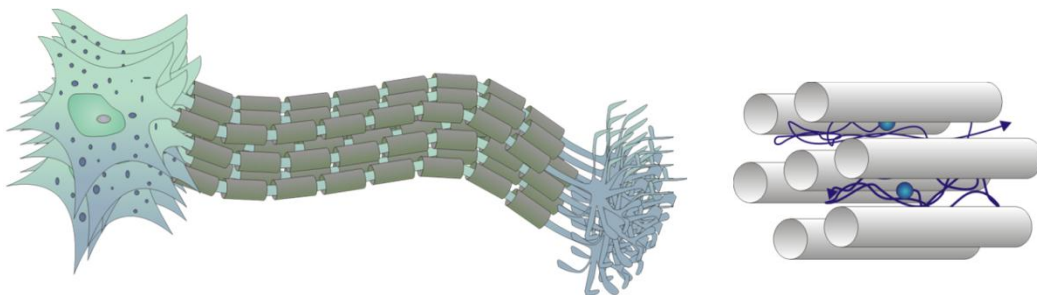
Figure 2.1 An axon bundle of neurons (left) and the hindrance of diffusion in directions perpendicular to axons (right) are shown. The figure is from Dr. Lajos R Kozák's presentation [16]

Diffusion of water in the white matter for cognitively normal people is considered to be highly anisotropic due to the underlying anatomical structure in the brain. White

matter is made up of the long fibres of neurons called axons. Axons form bundles which connect different parts of the grey matter of the brain. The structure of the bundles means that the diffusion of both intra- and extra-cellular water molecules is hindered in the directions perpendicular to the axons.

Because the integrity of the white matter structure is considered indicative of a person's cognitive condition the quantification of diffusion anisotropy in white matter may be descriptive of the progression of Alzheimer's disease. [28]

2.2   From DW MRI to DTI

The aim of diffusion-weighted (DW) MRI is to map the diffusion of water in biological tissues by measuring the attenuation of the MRI signal caused by diffusion. The signal attenuation caused in a particular gradient direction by DTI can be written as:

$$S_k = S_0 e^{-b\hat{g}_k^T D \hat{g}_k} \tag{2.3}$$

Where S_k is the measured DW signal in the kth gradient direction, S_0 is the signal measured without the diffusion weighting gradients and b is the characteristic value of the applied diffusion weighting gradients. $\hat{g}_k$ and $\hat{g}_k^T$ are the unit vector and its transposed in the direction of the applied kth diffusion weighting gradient. D is the diffusion tensor and $\hat{g}^T D \hat{g}$ defines a given component of the diffusion tensor as a projection. In order to map diffusion in 3 dimensions at least 6 + 1 MRI scans are required. 6 non-collinear scans are needed for the 6 independent components of the diffusion tensor. The additional scan is needed for the determination of S_0. A traditional approach is to acquire one image without DW and use a second value of b for the six non-collinear acquisitions, this way eliminating dependencies of relaxation factors prevalent during MRI scans. Nowadays, a higher number of gradient directions and b-values are used in order to improve the accuracy of the tensor estimation. From the rearrangement of equation (2.3) a particular component of the diffusion tensor can be expressed as:

$$D_{j,k} = \hat{g}_J^T D \hat{g}_k = \frac{\ln(S_0) - \ln(S)}{b} \tag{2.4}$$

DW images are most commonly performed using a single shot echo-planar-imaging (EPI) sequence modified to incorporate DW. The pulse sequence of the diffusion weighted EPI can be seen on figure 2.2. During EPI sequences a single slice of

a brain volume is acquired in one go. The idea behind using EPI sequences for DW imaging is to reduce patient motions during the scans. The gained speed in the acquisition is offset by the poor spatial resolution of EPI images compared to other types of acquisitions.
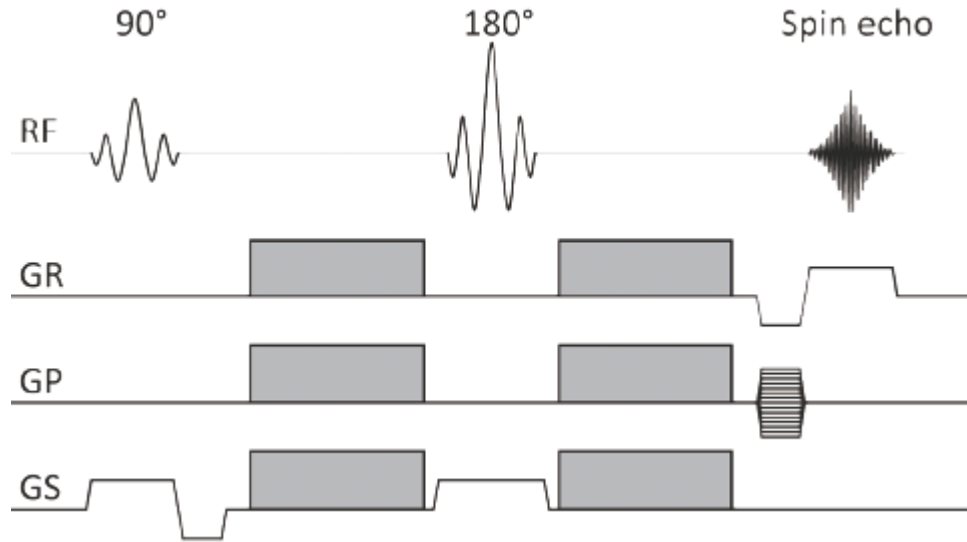
Figure 2.2 In this figure the abbreviation RF refers to the radio frequency pulses of 90 and 180 degrees used for EPI. Abbreviations GR, GP and GS stand for the readout gradient, the phase-encoding gradient and the slice-select gradient. The diffusion weighing gradient lobes can be seen coloured grey centred around the 180 degree RF pulse and can be applied in any gradient direction. The figure is from a study by P Winston [17]

2.3   Scalar measures of anisotropy

Several different measures can be derived from the diffusion tensor. This can be achieved by changing reference frames from the laboratory's [x y z] reference system defined by the MRI scanner into a voxel's local reference frame of [x' y' z'] where the principal component of the diffusion ellipsoid describing the anisotropy coincides with an axis. In such a reference frame the off-diagonal components of the tensor become zero. Such a reference frame change is achieved by the eigenvalue decomposition of the diffusion tensor. The tensor can be factorized as:

$$\boldsymbol{D} = \boldsymbol{E}^T \begin{bmatrix} \lambda_1 & 0 & 0 \\ 0 & \lambda_2 & 0 \\ 0 & 0 & \lambda_3 \end{bmatrix} \boldsymbol{E} \qquad (2.5)$$

Where $\boldsymbol{E}$ is a square matrix whose ith column contains the ith eigenvector and $\boldsymbol{E}^T$ is its transposed. λ_1, λ_2 and λ_3 are the corresponding eigenvalues to the eigenvectors as

4

components of a diagonal matrix. Local diffusion ellipsoids in each voxel are defined through equation (2.5).

$$\mathbf{D} = \begin{pmatrix} D_{xx} & D_{xy} & D_{xz} \\ D_{yx} & D_{yy} & D_{yz} \\ D_{zx} & D_{zy} & D_{zz} \end{pmatrix} = \mathbf{E}^T \begin{pmatrix} \lambda_1 & 0 & 0 \\ 0 & \lambda_2 & 0 \\ 0 & 0 & \lambda_3 \end{pmatrix} \mathbf{E}$$

Tensor derived from directional diffusivities (ADC's)   Eigenvalues   Matrix of 3 eigenvectors
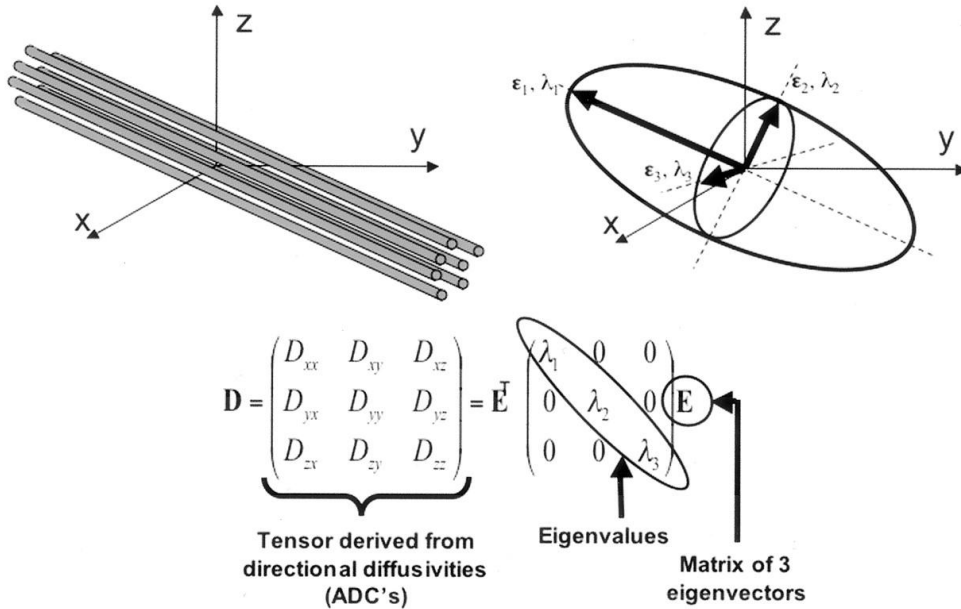
Figure 2.3 Top left: Fiber tracts orientation shown in relation to laboratory reference frame. Top right: The 3 dimensional diffusion modelled as an ellipsoid shows how eigenvectors and values define this ellipsoid. Bottom: Derivation of tensor decomposition is shown. The figure is from a study by J. Jellison et al [18]

Numerous scalar measures have been devised to quantify the anisotropy ellipsoid. [22] For my thesis I used the fractional anisotropy (FA), mean diffusivity (MD), radial diffusivity (RD) and axial diffusivity (L1). Each of the four metrics are defined from the eigenvalues of the diffusion tensor.

$$FA = \sqrt{\frac{3}{2}} \sqrt{\frac{(\lambda_1 - MD)^2 + (\lambda_2 - MD)^2 + (\lambda_3 - MD)^2}{\lambda_1^2 + \lambda_2^2 + \lambda_3^2}} \qquad (2.6)$$

$$MD = \frac{\lambda_1 + \lambda_2 + \lambda_3}{3} \qquad (2.7)$$

$$L1 = \lambda_1 \qquad (2.8)$$

$$RD = \frac{\lambda_2 + \lambda_3}{2} \qquad (2.9)$$

Where λ_1 is the principal eigenvalue and λ_2 and λ_3 are the two other eigenvalues whose eigenvectors are perpendicular to the principal eigenvalue's eigenvector. The FA metric takes up values between 0 and 1 and quantifies how elongated the diffusion ellipsoid is. 1 being when $\lambda_1 \gg \lambda_2 \gg \lambda_3$ (high level of anisotropy) and 0 being the case of isotropic diffusion (sphere): $\lambda_1 = \lambda_2 = \lambda_3$.

2.4 VBA methods

Two main approaches of VBA are the TBSS method and the whole brain VBA method.

The TBSS method is heavily reliant on the fractional anisotropy (FA) DTI metric and can be summarized through Figure 2.4. In the TBSS pipeline FA images are co-registered to a template then averaged to form a "skeleton" image. The FA-skeleton is formed from the centres of major white matter tracts that are present in all of the subjects. For the tracts only skeleton voxels with FA higher than a threshold value are included. Then each subject's spatially normalized FA image is projected onto the skeleton image. Transformations can also be applied to additional DTI parameter maps. One major drawback to TBSS is the possibility of the loss of relevant data in the skeletonization step. [5]
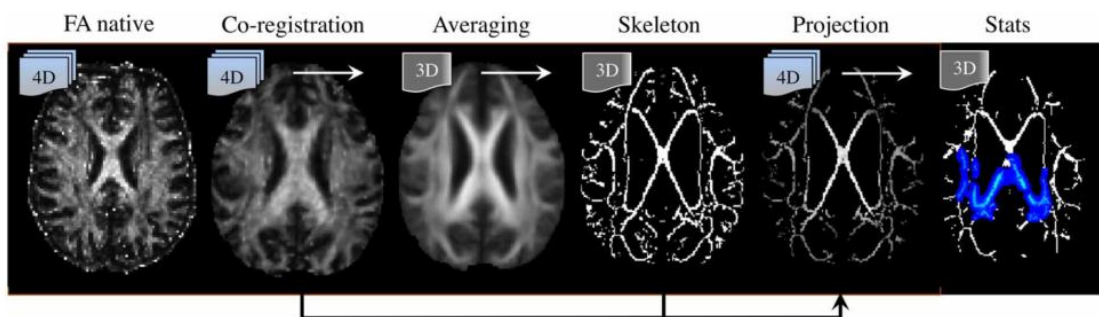
Figure 2.4 Summarization of the steps in the TBSS pipeline. Figure from the study by J Acosta-Cabanero [5]

In contrast to TBSS the whole brain method relies less on FA. After spatially normalizing each subject into common space, smoothing is applied to increase the statistical power of results. The actual implementation of this method is discussed in-depth in later chapters.

3   Alzheimer's disease

Alzheimer's disease (AD) is the most common form of dementia, as around 70% of dementia cases can be attributed to AD. AD is chronic neurodegenerative disease that causes the brain to deteriorate over time starting slowly and getting worse gradually. The initial advancement of AD is often characterized by the loss of the patient's short-term memory. Exact diagnosis can often only be made posthumous. As the disease progresses gradually bodily and social functions of the patient are completely lost. Intensive caretaking of patients with AD is expected by the end of the disease. Currently there are no known cures of the disease. [3]

Due to AD's great socio- and economic burdens on society, intensive research is currently being conducted. As a result large well documented multi-modal databases of patients in various phases of the progression of AD have been set up world-wide to help focus research. One such initiative is the Alzheimer's Disease Neuroimaging Initiative (ADNI). [8]

One of the primary aims of research today is the development of non-invasive diagnostic techniques that can allow diagnosis at early progression. Traditionally AD was considered as a disease of the grey matter, but recent developments in the field have revealed that white matter structural integrity can also be indicative of the progression of AD. Recent studies have suggested that white matter atrophy in AD can be more than just a secondary effect of the experienced atrophy of the grey matter. [28]

Currently the two most accepted theories in the scientific community as the causes of AD are the amyloid and the tau hypotheses. The amyloid hypothesis explains AD with extracellular deposits of amyloid-β plaques around nerve cells. These plaques are responsible for inhibiting the communication of nerve cells and thus causing the atrophy. The tau hypothesis explains AD as the intracellular effects of tau proteins. The tau proteins form neurofibrillary tangles inside the cells that cause the microtubules of the cell's cytoskeleton to disintegrate. This leads to the eventual destruction of the nerve cell. [23]

3.1 ADNI

The Alzheimer's Disease Neuroimaging Initiative (ADNI) is a North American and Canadian initiative established to develop a database of normal subjects (CN), subjects with mild cognitive impairment (MCI), and subjects with mild Alzheimer's disease (AD) registered using standardized imaging techniques of various different modalities. [8]

Altogether 227 patients were identified with available baseline scans of both T1 weighted (T1w) and diffusion weighted (DW) MRI scans for my sample. Patients that passed quality controlling of their scans are summarized in table 3.1. A subgroup was created out of the original sample where baseline results for PET scans and volumetric results from MRI scans were available. These results have been summarized in table 3.1 along with figures 3.1 and 3.2 showing the age distributions of the original sample and the subgroup. The classification of patient's mental health condition was also acquired from the ADNI database.

Groups	Initial sample size	Mean age [year]	Standard deviation		Reduced sample size	Mean age [year]	Standard deviation
CN	80	75.6	5.7		71	75.8	5.8
MCI	88	76.4	6.9		79	76.6	6.9
AD	49	77.7	8.7		39	77.6	9.1

Table 3.1. The number of subjects in each group. The second column is after correcting for badly normalized subjects. The fifth column is after correcting for the availability of subjects PET and volumetric ratio scores.

Mini–mental status examination (MMSE) and Rey Auditory Verbal Learning Test (RAVLT) psychological assessment scores were also extracted from the ADNI database for all subjects. The MMSE is a test used both clinically and in reasearch to measure cognitive impairment on a 30 point scale with the higher scores corresponding to healthier subjects.[24] RAVLT is psychological memory assessment aimed at evaluating verbal memory function of subjects. For this assessment the Immediate recall part was extracted for subject which measures memory dysfunction on a 0 to 75 scale with higher scores corresponding to healthier subjects.[25]
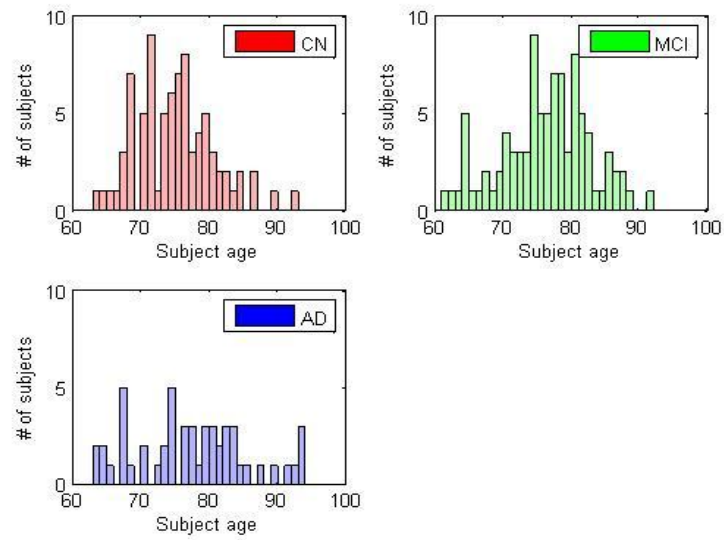
Figure 3.1 The age distributions of the three subject groups for the initial sample size. The mean and standard deviation of each distribution can be found in table 3.1.
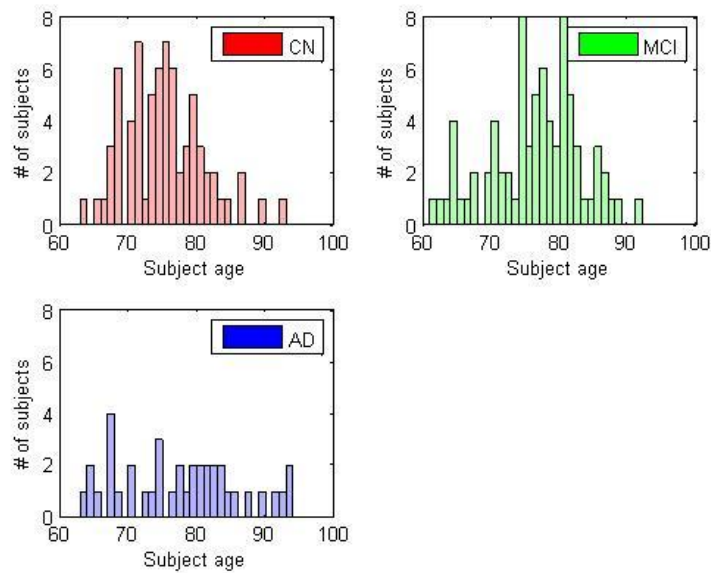

Figure 3.2 The age distributions of the three subject groups for the reduced sample size. The mean and standard deviation of each distribution can be found in table 3.1.

4 DTI metrics and white matter microstructure in Alzheimer's disease

Previous results from the corresponding literature suggested decreased values of FA and increased MD values in most white matter regions of the brain in AD. Exceptions of this trend however included parietal and internal capsule white matter regions for the FA metric. Exceptions also included parietal and occipital lobes in case of the MD metric. [6]

An example of significant results found with TBSS can be seen on Figure 4.1. Highlighted areas show where statistically significant differences occurred between groups CN and AD. The TBSS results also provided a platform to validate or possibly contradict results gained from the whole brain VBA method implemented in this thesis.
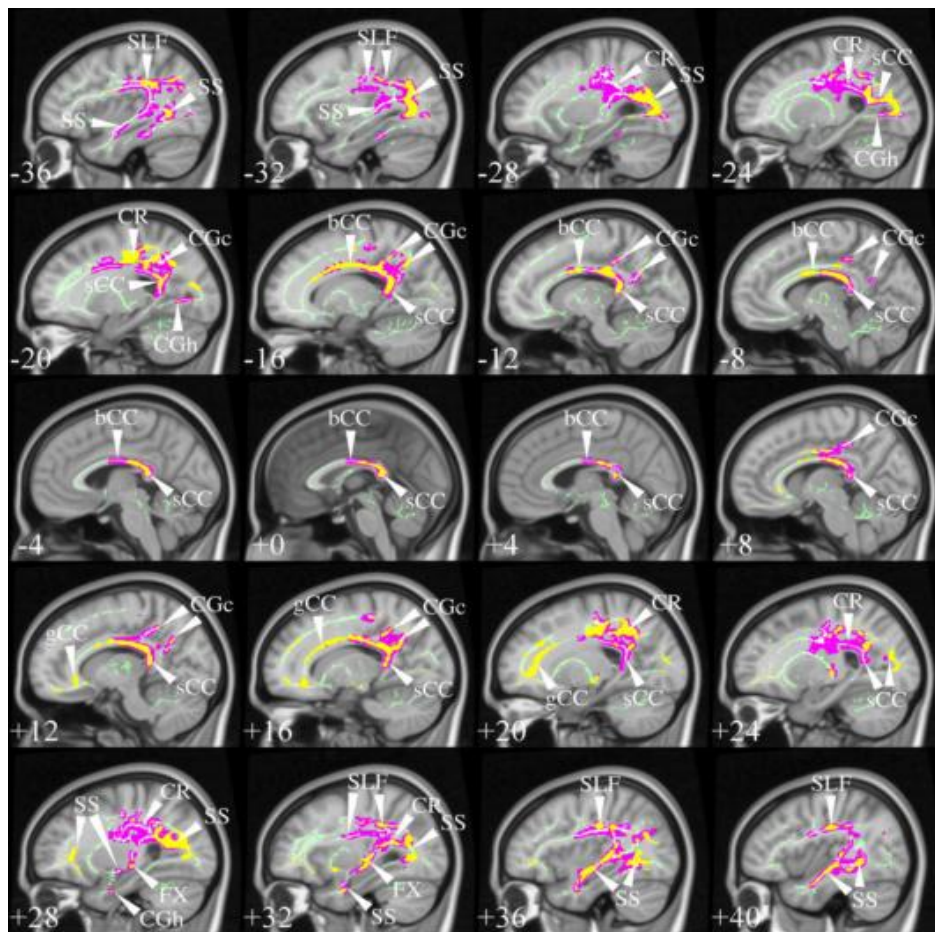
Figure 4.1 Results gained from a TBSS study with pink clusters denoting increased mean diffusivity (MD) areas yellow clusters represent anisotropy (FA) reductions for AD patients at p < 0.05 controlled for the multiple comparisons problem. The relevant areas highlighted are: [SLF] superior longitudinal fasciculus; [SS] sagittal stratum; [CR] corona radiata; [s/b/gCC] splenium/body/genu of the corpus callosum; [CGc/h] cingulum at the level of the posterior cingulate/parahippocampus; and [FX] fornix. Figure from the study by J Acosta-Cabanero [5].

5 General linear model (GLM)

The general linear incorporates a number of different statistical models. For my thesis such models included Student's t-test, analysis-of-covariance (ANCOVA) and the F-test for the analysis-of-variance (ANOVA). The general linear model explains the dependent variable Y_i (the results of a measurement) as a linear combination of independent explanatory variables and an error term of ε_i :

$$Y_i = x_{i1}\beta_1 + x_{i2}\beta_2 + \ldots + x_{ij}\beta_j + \ldots + x_{iN}\beta_N + \varepsilon_i \qquad (5.1)$$

where $i = 1, \ldots M$ is the index of observations. For each dependent variable i there exists a set of N (N < M) independent variables x_{ij} where $j = 1, \ldots, N$. The β_j are the parameters to be estimated for each of the N independent variables of x_{ij} . The error terms ε_i are considered to be normally distributed random variables.

Equation 5.1 can be written as a matrix equation:

$$\boldsymbol{Y} = \boldsymbol{X\beta} + \boldsymbol{\varepsilon} \qquad (5.2)$$

Where $\boldsymbol{Y}$ is the column vector of the dependant variables, $\boldsymbol{\varepsilon}$ is the column vector of error terms, $\boldsymbol{\beta}$ the column vector of parameters to be estimated and $\boldsymbol{X}$ is an M x N matrix called the design matrix consisting of the x_{ij} independent variables. The x_{ij} independent variables may be dummy variables or covariates.

5.1 Dummy variables

Dummy or categorical independent variables are used to represent categories or levels of a given factor for an experiment. Because dummy variables cannot be entered directly into the GLM the alternate method of dummy coding is done. The dummy variables are included in the design matrix which can take on values of 0 or 1 to indicate the absence or the presence of a categorical independent variable. Equation (5.3) shows a dummy coded design matrix for an experimental factor which has two levels.

$$Y= \begin{pmatrix} 1 & 0 \\ 1 & 0 \\ \vdots & \vdots \\ 1 & 0 \\ 1 & 0 \\ 0 & 1 \\ 0 & 1 \\ \vdots & \vdots \\ 0 & 1 \\ 0 & 1 \end{pmatrix} \begin{pmatrix} \beta_{group1} \\ \beta_{group2} \end{pmatrix} + \varepsilon \qquad (5.3)$$

5.2 Covariates

Covariates can be considered as independent continuous or discrete variables added to the design matrix in order to improve the GML model. Equation (5.4) shows a dummy coded design matrix with a covariate included in the modelling of the experiment. The adding of the covariate r to the model also adds a component to the estimated parameter vector.

$$Y= \begin{pmatrix} 1 & 0 & r_1 \\ 1 & 0 & r_2 \\ \vdots & \vdots & r_3 \\ 1 & 0 & r_4 \\ 1 & 0 & r_5 \\ 0 & 1 & r_6 \\ 0 & 1 & r_7 \\ \vdots & \vdots & r_8 \\ 0 & 1 & r_9 \\ 0 & 1 & r_{10} \end{pmatrix} \begin{pmatrix} \beta_{group1} \\ \beta_{group2} \\ \beta_r \end{pmatrix} + \varepsilon \qquad (5.4)$$

5.3 Contrasts

In statistics contrasts can be vectors or matrices of weights used to express hypotheses as a linear combination of the estimated parameters contained in the $\boldsymbol{\beta}$ vector and the contrast. For example in the case of a two sample t-test the null hypothesis of $H_0: \boldsymbol{c\beta} = 0$ with a contrast vector of $[1 \ -1]$ can be expressed as the t statistic of:

$$t = \frac{\boldsymbol{c\beta}}{S_\beta} = \frac{\beta_1 - \beta_2}{S_\beta} \qquad (5.5)$$

Where S_β is the weighted sum of the individual standard deviations of each β_i component. This t-test will test whether the effects of the parameter estimate β_1 are greater than those of in β_2.

5.4   Statistical tests: Student's t-test and the F-test

In statistics two-sample t-tests are used to determine whether the sets of data are significantly different from one another by the calculation of the t statistic as mentioned in equation (5.5). For a given significance level of α the calculated t statistic is compared to a t-distribution of $N - k$ degrees of freedom. For my particular case N was the number of dependant variable components in Y and $k = rank(X)$, was the rank of the design matrix of the GLM. Then a p-value can be calculated from the t distribution and compared with the significance level of α. Depending on whether the p value is smaller or greater than α the null hypothesis is rejected in favour of the alternative hypothesis or the null hypothesis cannot be rejected. In this case the alternative hypothesis is that the means of the two samples are significantly different.

In case one wants to compare more than two groups the ANOVA, a generalization of the t-test, is needed. ANOVA uses the F-test to assess whether estimated parameters of two or more groups differ from each other. When there are only two means to compare, the t-test and the F-test are equivalent and the relationship between the two statistical scores is:

$$F = t^2 \qquad (5.6)$$

The F-test for ANOVA can be thought of as a ratio of the between and the within group variance:

$$F = \frac{between\ group\ variance}{within\ group\ variance} \qquad (5.7)$$

The disadvantage of the F-test is that if the null hypothesis is rejected it is not clear which of the group or groups are significantly different from the others. Similarly to the t-test the F-test can also be formalized with the use of a contrast matrix. The exact derivation of this can be found in "*The Human brain function*" [2]

5.5 ANCOVA

The ANCOVA is a special case of ANOVA where the statistical power is increased by reducing the within group variance in equation (5.7) by controlling for the effects of covariates. Because covariate effects can be explained by the within group variance the removal of this in the denominator of equation (5.7) will lead to a larger value of the F statistic. This can be useful in cases when the added covariate accounts for only a very little variance in the dependent variable and therefore might actually reduce power of the ANOVA without controlling for covariates.

5.6 Multiple comparisons problem

In fields like neuroimaging simultaneously many thousands of tests are performed at once when comparing different groups of subjects on a voxel-wise basis. A single statistical test is conventionally considered significant if a certain p-threshold of α is not exceeded. Problems occur when multiple tests are being evaluated at a set α for statistical significance. For example taking an estimate of having 100 000 voxels in the brain being compared with a significance level at $\alpha = 0.05$. On average 5000 of the voxels will be false-positive, i.e. where the null hypothesis was falsely rejected. To correct for false positives the p-threshold of α needs to be adjusted to account for the number of tests being performed. This correction in SPM is done using a multiple step process called random field theory (RFT) which corrects for the so called family-wise error rate (FWER). [2] FWER expresses the probability of having at least one false positive among the multiple comparisons performed. The RTF method can be considered a less conservative one than other correction methods of the FWER such as the Bonferroni correction where the significance level is divided by the number of tests being performed. [27]

6   DTI processing pipeline

In this chapter of the thesis I would like to give an overview of what steps were involved in the processing pipeline of converting the raw diffusion weighted images into normalized DTI parameter maps. The goal of spatial normalization was to overcome individual differences of each subject's brain and to deform the images so that one voxel in one subject's image corresponded to the same voxel in another subject's image.

The two components needed for the normalization procedure were the T1w anatomical images and the DW images. The pre-processing of the images for normalization was done with Alexander Leemans's ExploreDTI [26], a Matlab based software. The co-registration of the two modalities and the spatial alignment of the DTI parameter images into a common space was done with University College London's SPM12 [15], another Matlab based software package. Statistical parametric mapping (SPM12) is most commonly used for the analysis of functional MRI (fMRI). 2nd level analysis in SPM used for the statistical evaluation of fMRI data could also be used on DTI data.

6.1   Converting DICOM images to NIFTI Images

The first step for the 2 modalities was to convert the raw DICOM files into a so called NIFTI *(*Neuroimaging Informatics Technology Initiative*)* data format. [11] NIFTI is currently the most widely used file format for neuroimaging software such as ExploreDTI and SPM12.

The conversion was done with the help of Chris Rodent's dcm2nii software. [11] During the conversion of the DW DICOM files along with the image volumes being converted into one NIFTI file the gradient directions and b-values of the applied gradients were also extracted into separate files.

6.2   Preprocessing of T1w images

The preprocessing of T1w images was needed as a template for the correction of EPI and eddy-current distortions of the DW images. The steps for this were done with ExploreDTI along with an additional semi-automated volume cropping Matlab script written by myself. The cropping script was needed to reduce the size of the non-skull stripped T1w images. This meant removing the non-relevant data left on the scans, such as the neck of each subject and larger empty background areas. Erasing these allowed computations to run faster for the proceeding normalization steps.

The cropping of volumes was followed by flipping the axes of the T1w images transforming them into ExploreDTI's coordinate system. The flipping procedure was followed by masking in which background areas were zeroed out.
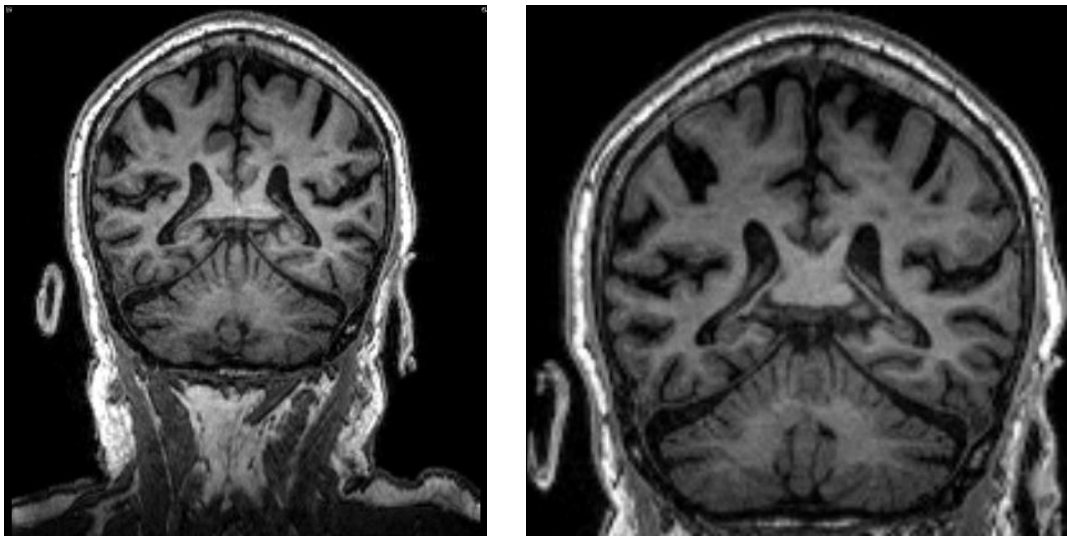
Figure 6.1 The effects of the semi-automated cropping script can be seen. Thresholding in the inferior direction was done manually by specifiyng the z coordinate at the base of the cerebellum for each subject.

6.3   Correcting of DW images and exporting DTI metrics

With preprocessed T1w images used as a reference, EPI and eddy-current corrections to the DW images could be performed.

DW scans are acquired using EPI sequences as mentioned in chapter 2.2. Because EPI pulse sequences are very sensitive to B0 field inhomogeneities geometric distortion artifacts are likely to appear on acquired images. An example of this is illustrated in figure 6.2 .

During DW acquisition, problems with induced eddy currents arise when strong gradient pulses are switched rapidly on and off during the pulse sequence. The time-varying magnetic field of the gradients results in inducted eddy currents in the various conducting surfaces of the rest of the MRI scanner. These, in turn, set up magnetic field gradients that may persist after the primary gradients are switched off and can result in significant direction-dependent distortions in the acquired images. Such distortions can be seen in figure 6.2.

For the actual implementation of these corrections I used Mark Drakesmith's suggested steps [12] for achieving optimal correction results with ExploreDTI.
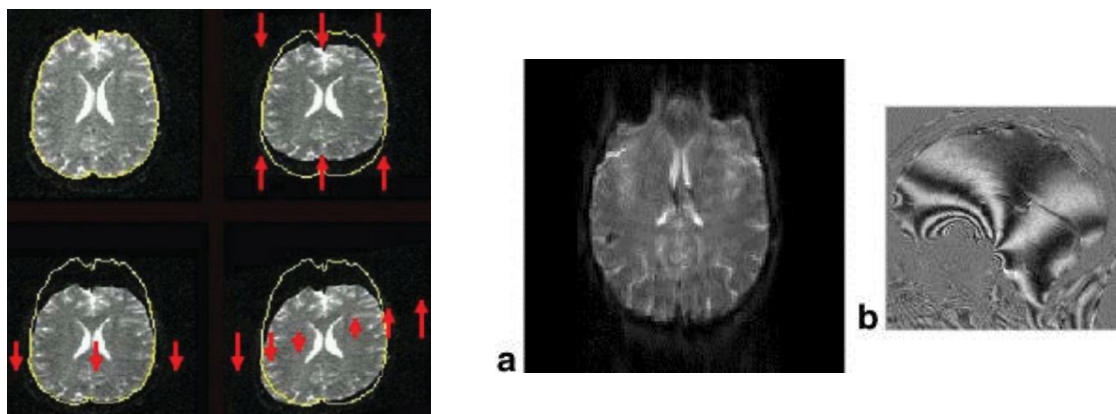
Figure 6.2 Artifacts as a result of eddy currents can be seen on the left. The images on the right a) show the effects of geometric distortions induced by magnetic susceptibility differences.in the frontal lobe of the brain tissue, bone, and air-filled sinuses. Image b) is a phase map showing the B0 field inhomogeneities. Such phase maps can be used to correct for the geometric distortions. Figures from the study by Le Bihan et al. [19]

After the corrections the fitting of the tensor model could be completed on the DW images and the FA, L1, MD and RD metrics were exported from the tensor model as separate parameter maps.

6.4 Spatial normalization with SPM12

Tissue segmentation was applied on the Tw1 images for the separation of grey matter, white matter and areas containing cerebrospinal fluid. As a result of the segmentation each voxel was assigned a probability value representing the corresponding tissue type it belonged to. The assignment of probabilities to voxels was done using the intensity distributions of each image and prior information about the tissue classes. The a-priori information was available in SPM from a large sample of correctly segmented images. The determination of the tissue type from values of an image histogram can be seen on Figure 6.3. The incorporation of prior information into the identification of the type of tissue can be seen on Figure 6.4. The result of such a segmentation was used in the creation of a white matter mask to limit the calculation to white matter voxels when performing statistical analyses of the FA metric.

Because the T1w images provide a much higher anatomical resolution, the segmentation, which also yielded the transformations to align each subject's data into the normalized space was performed on them. Since the correction of the DWI-images also meant coregistering them to the T1w images, the subject's corresponding DTI–parameter images could be transformed with the same transformation matrices. The common coordinate system into which the normalization was performed was the so called MNI space (Montreal Neurological Institute). [13] The MNI space is a predefined coordinate system in which various brain atlases have been defined from large series of MRI scans on cognitively normal subjects.
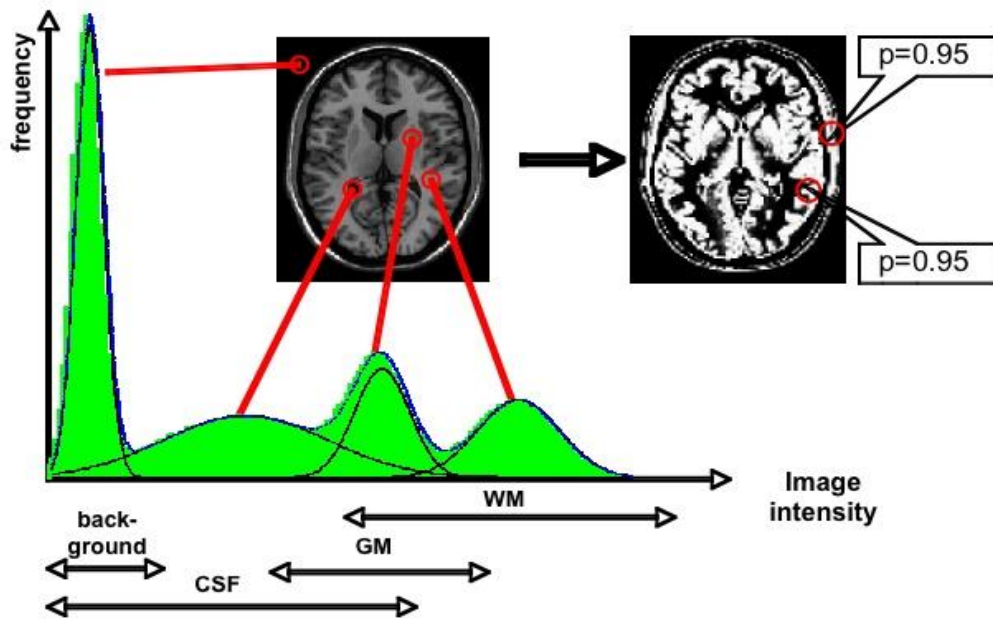
Figure 6.3 Distributions belonging to each tissue of the different tissue types and the background can be identified from the histogram of an image. The horizontal axis shows image intensities increasing from left to right. The top right image highlights the need for prior information in determining the tissue type. Here part of the skull can be seen falsely registered grey matter. The figure is from the University of Lena's structural brain mapping group's homepage. [20]
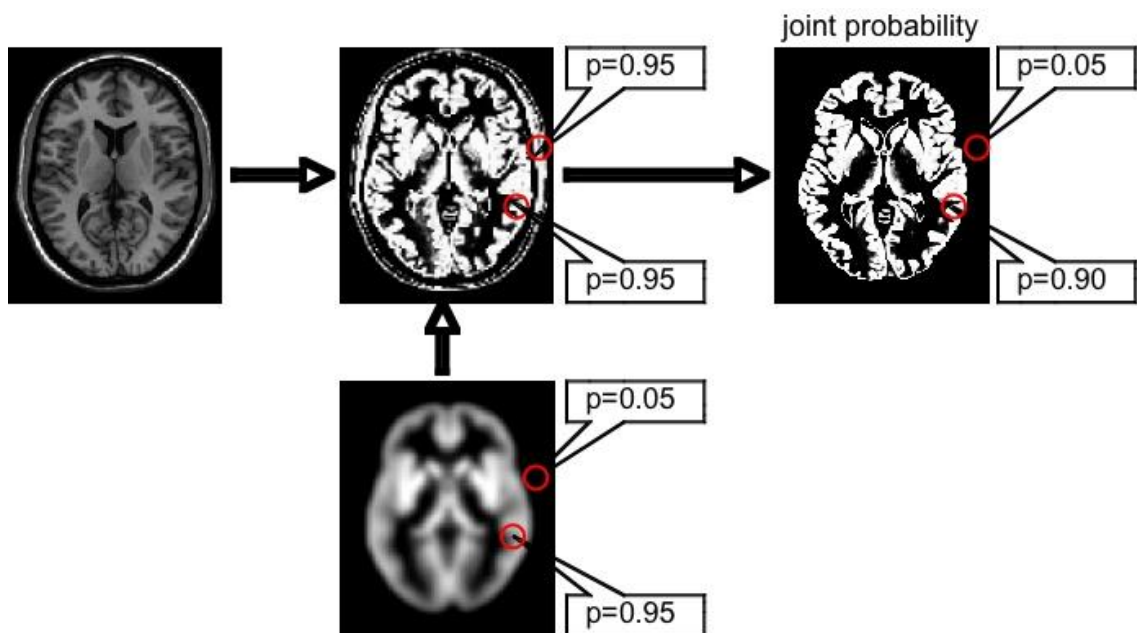

Figure 6.4 The use of prior knowledge about the tissue types are encoded into the identification of tissue type for the T1w structural images. Figure from University of Lena's structural brain mapping group's homepage The figure is from the University of Lena's structural brain mapping group's homepage. [21]

6.5   Smoothing

The purpose of spatial smoothing was to the increase statistical power by reducing the effects of normal anatomical variabilities still present after the normalization step. It is also a way to improve the signal-to-noise ratio due to the averaging effects of smoothing. Smoothing was applied as a spatial Gaussian convolution filter on the DTI data.

The exact effect of spatial smoothing on statistical power is not straightforward. By smoothing not only is the signal to noise ratio of each voxel increased, but also the number of voxels that are considered independent of each other are reduced.
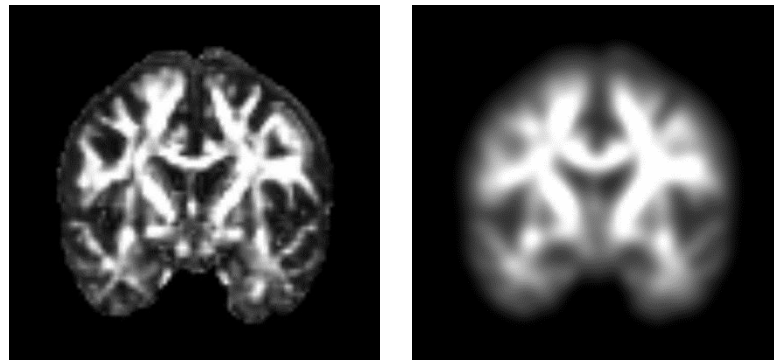
Figure 6.3 FA maps of a subject with and without application of smoothing can be seen.

7   Statistical analysis of the DTI data

In this chapter I would like to discuss the results I obtained from the statistical analysis of my normalized DTI data. I performed several single factor analyses between-subjects in order to test for significant differences between the CN, MCI and AD groups. The factor was each subject's cognitive condition which could be characterized by the 3 levels.

All performed statistical analyses in this thesis, except for the region-of-interest (ROI)-level correlation analysis, are between-group analyses performed on a voxel-wise whole brain level.

The two most commonly investigated DTI metrics are the FA and the MD. Likewise, our analyses were also performed on these two.

All of figures in this chapter are in neurological convention meaning the left side of the subject's brain is on the left side of the MRI image.

Throughout the statistical analysis only smoothed parameter maps of metrics were used in order to increase the statistical power of results. Parameter maps were smoothed with a 3D Gaussian convolution mask with a full width at half maximum (FWHM) of 8 mm.

Throughout my statistical analyses whenever normalized subjects were compared in a voxel-wise fashion, results for the correction of the multiple comparisons problem were investigated. In SPM12 p-thresholds are corrected for by the FWER using the RFT correction method. A corrected value of $p < 0.05$ implies that the probability of a false positive occurring in all of the tests performed is controlled at 5%. [15]

With SPM differences in measured DTI metrics between groups are shown as coloured patches overlaid on MRI images. The patches represent the location of voxels that have shown statistically significant differences between groups and gradient of colours are mapped to the each significant areas statistical scores. The colour bars on the figures (for example figure 7.6 (b)) represent the range onto which the mapping of the scores was done.

7.1 Masking

Initial statistical investigations showed the FA metric to contain a large amount of noise in the grey matter areas of the brain. Explicit masking was applied throughout the analysis conducted with statistical tests on this metric in order to reduce this noise. An example of this can be seen on Figure 7.1 which shows significant differences with and without the application of masking the white matter regions of the brain.
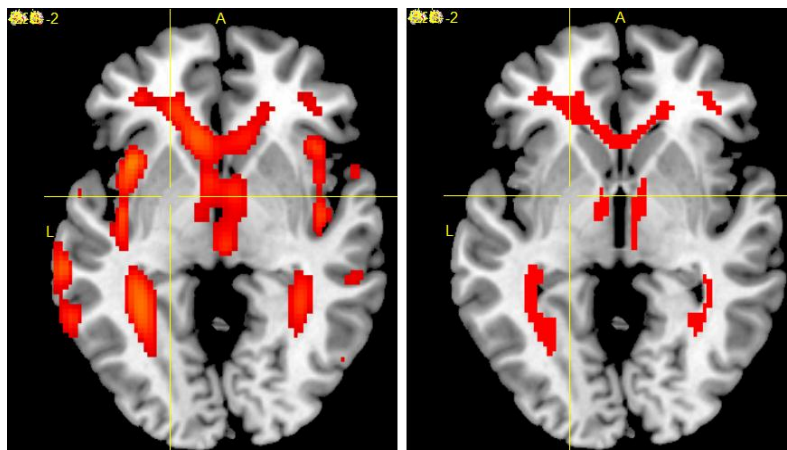
Figure 7.1 Results for FA can be seen with (right) and without (left) the application of masking the white matter regions.

Such a mask was created from an averaged white matter template. White matter regions of each subject's image were available from the segmentation process completed during spatial normalization of the DTI images. In Figure 7.2 a white matter mask can be seen created from an averaged white matter template threshold set at a probability of 0.5.
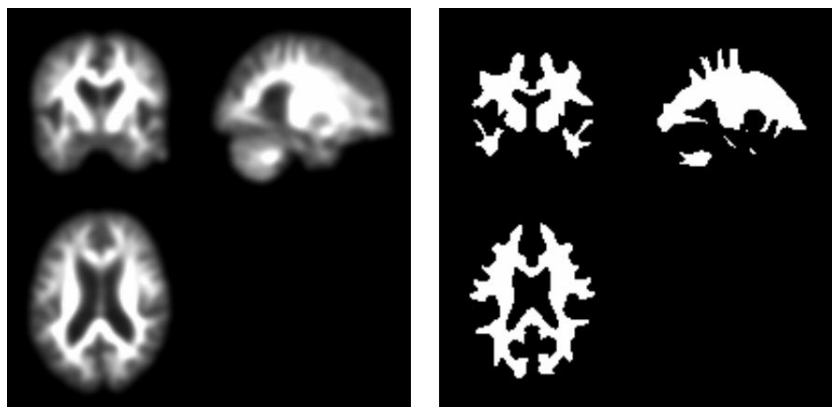
Figure 7.2 Averaged white matter template (left), and the resulting white matter mask (right) from applying the threshold to the template.

7.2 ANOVA

The first of the group statistics I investigated was a single-factor 3-level ANOVA. As discussed in chapter 5.4 the ANOVA provides a statistical framework for testing for significant differences in 2 or more groups by F-tests. The drawback of the F-tests are that one can only predict whether or not there are significant differences in one or more of the levels but cannot determine which of level or levels differ.

Given that the ANOVA is an exploratory data analysis it was a suitable candidate for first analysis performed on my sample. For the F-test in my particular case I needed a contrast that would allow me to compare groups CN, MCI and AD against one another. The null hypothesis of the F-test for a particular DTI metric was:

$$H_0: \beta_{CN} = \beta_{MCI} = \beta_{AD} \qquad (7.1)$$

As there are 2 equals signs in equation (7.1) the F-contrast is defined by 2 equations: $\beta_{CN} = \beta_{MCI}$ and $\beta_{MCI} = \beta_{AD}$. By setting each equation to zero one can determine the relevant contrast coefficients. In case of the first equation one gets the following contrast vector:

$$\beta_{CN} - \beta_{MCI} = 0 \ \rightarrow \ \begin{bmatrix} 1 & -1 & 0 \end{bmatrix} \qquad (7.2)$$

Keeping in mind that all other coefficients of the contrast vector (whether belonging to another group or covariate) are equal to zero. It is also important to note, that as mentioned in chapter 5.4 there is only need to define the contrast in one "direction" as the F-test is sensitive for significant differences in both "directions". The corresponding alternative hypothesis for equation (7.1) is:

$$H_{alternative}: \beta_i \neq \beta_k \qquad i \neq k \qquad (7.3)$$

where $i, k = CN, MCI, AD$.

Combining the two contrast vectors as one F-contrast matrix one gets:

$$c_{F-test} = \begin{bmatrix} 1 & -1 & 0 \\ 0 & 1 & -1 \end{bmatrix} \qquad (7.4)$$

Using equation (7.4) as my contrast, the three groups exhibited significant differences in FA and MD (figure 7.6). The most prominent differences in the three groups' means were visible in the case of the MD metric. The highlighted white matter

brain regions are the temporal lobes, as shown in as shown in figure 7.6(a). Figure
7.6(b) shows the whole of the corpus callosum as a significantly differing area where
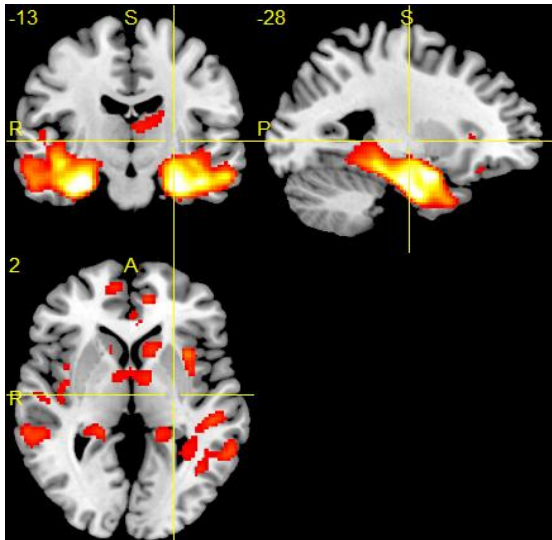the H_0 was rejected for the ANOVA.

Figure 7.6. (a) Results for MD with the F-contrast of equation (7.4) with a corrected p value.
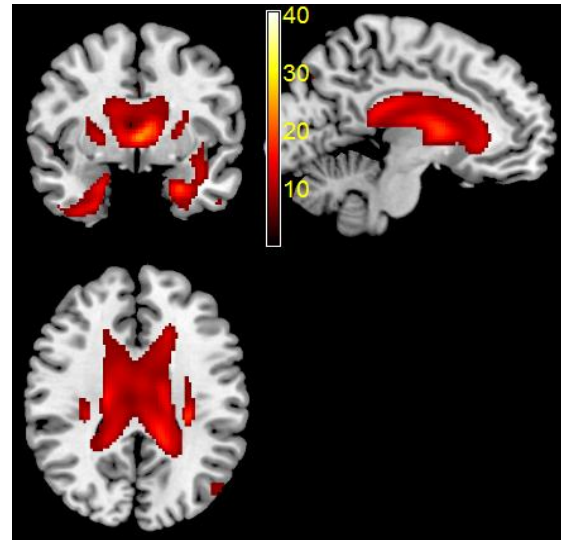

Figure 7.6. (b) Results for the FA metric with the F-contrast of equation 7.4. with an uncorrected p value.
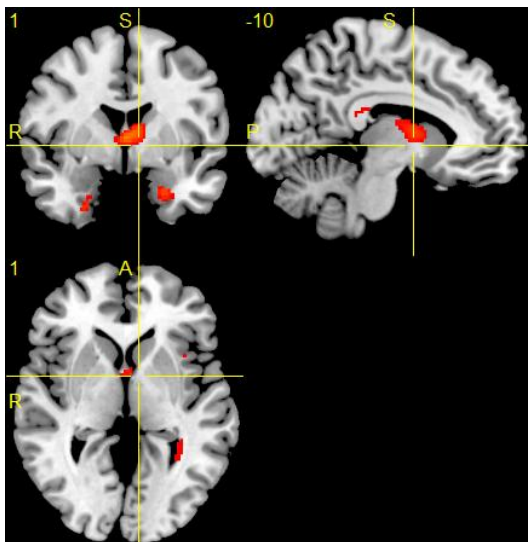

Figure 7.6. (c) Results for the FA metric with the F-contrast of equation (7.4) with a corrected p value.

Figure 7.6 Results in (a) are of the One-way ANOVA for the MD metric with the significance level set to p<0.05 and corrected for multiple comparisons. Results of the One-way ANOVA for the FA with an uncorrected (b) p-value of p <0.001 and corrected p-value for multiple comparisons of p< 0.05 in (c). The colorbar in in figure 6.4 (b) represent the range in which the linear mapping for the F satistics was done in all three cases.

7.3   Statistical analysis with two-sample t-tests

For an in-depth analysis as to which of the subject groups differed in their mean from the other groups unpaired two-sample t-test were required. I expected to see the most significant differences between the CN and AD groups as the structural changes in white matter since these are the two groups that differ most in their level of Alzheimer's disease.

To improve the GLM model each subject's age, handedness and gender were taken into consideration as covariates in the design matrix for the whole sample. A further covariate added in case of some of the subjects was their baseline results of a derived volumetric ratio. The volumetric ratio was calculated as the ratio of the intracranial volume of the brain and the whole brain volume.

Setting up contrasts in the cases of the different metrics for the t-tests was very similar to the way discussed in chapter 7.2. The only notable difference was that instead of a matrix the contrast was simply expressed as a vector of coefficients. Unlike the one-way ANOVA the nature of the t-test required each comparison to be made in "both" ways, as the sign of the coefficients would result in a different hypothesis being tested. The expectations in contrasts vectors differed slightly for of the four DTI-metrics:

- Mean FA values were expected to be smaller in subjects with AD as a result of the disintegration of structure. This required a contrast vector of [1 -1] where the two contrast coefficients to group CN and AD or CN and MCI respectively.

- The opposite was expected in the case of MD with the progression of Alzheimer's, meaning I expected to see higher mean values of MD in voxels of the AD group. This meant a contrast vector of [-1 1] where the contrast coefficients to group CN and AD or CN and MCI respectively.

- In case of the RD and L1 the expectation was similar to that of the MD. Meaning that with the progression of Alzheimer's the mean values for these two metric would increase as well.

In general the null hypothesis for the performed t-tests could be formulated as:

$$H_0: \beta_i = \beta_k \qquad i \neq k \qquad (7.5)$$

The corresponding alternative hypothesis for H_0 was:

$$H_{alternative}: \beta_i \neq \beta_k \qquad i \neq k \qquad (7.6)$$

In both equations 7.5 and 7.6 $i, k = CN, MCI, AD$.

Initially I investigated to see whether any significant differences between the CN and the MCI group means were visible. Results for this can be seen in figure 7.9. Results in figure 7.9 showed significant differences in the region of left temporal lobe in the case of MD.
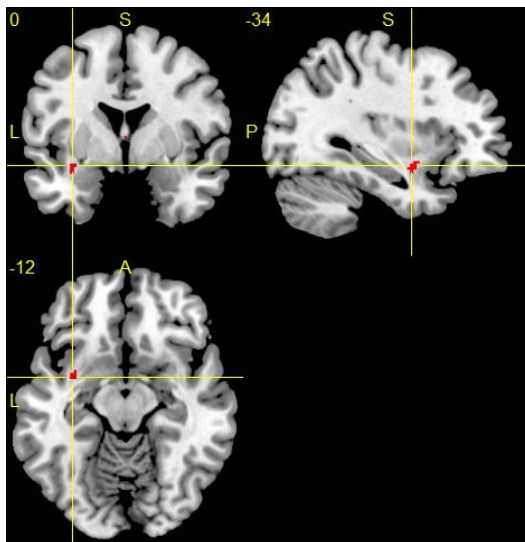

Figure 7.9 (a) results for brain regions where mean FA values for voxels is higher in the CN group.
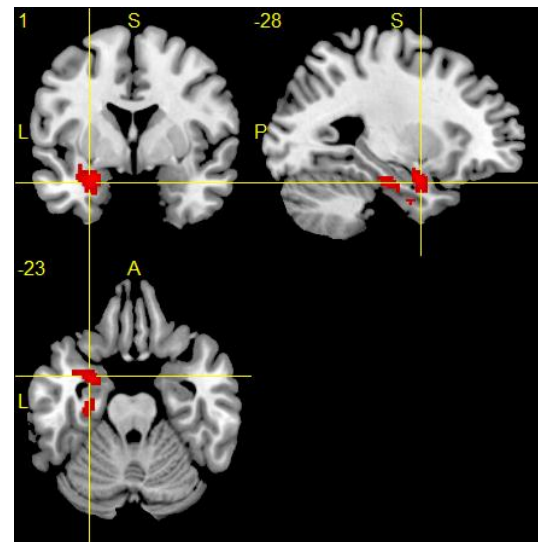
Figure 7.9 (b) results for brain regions where mean MD values for voxels is higher in the MCI group.

Figure 7.9 Results of comparing CN and MCI groups for MD and FA can be seen on figures (a) and (b). For figure (a) p < 0.001 without correction for multiple comparisons. For figure (b) p < 0.05 is corrected for multiple comparisons.

I also performed t-tests on each of the four metrics to compare groups CN and AD. The results of these tests can be seen in figure 7.14. Significant differences could be seen in the corpus callosum similarly to what the one-way ANOVA results gave for the FA-comparison (figure 7.6).
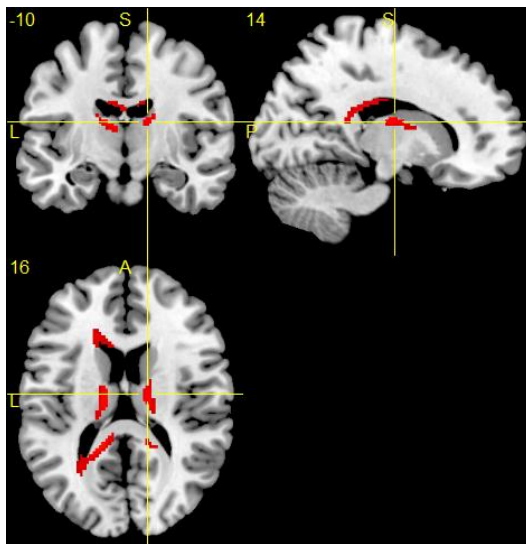
Figure 7.14 (a) results for brain regions where mean FA values are higher in the CN group.
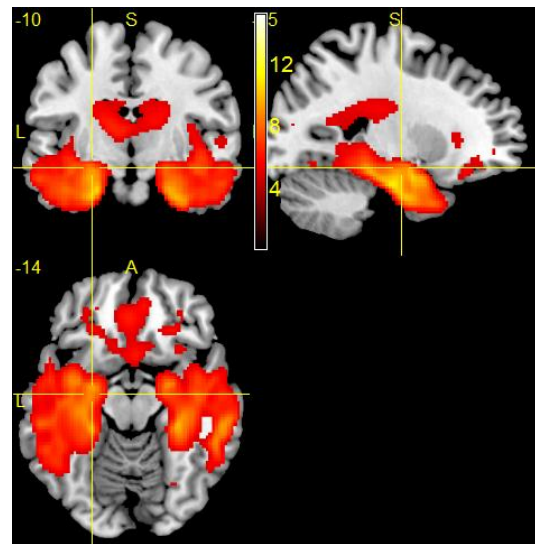

Figure 7.14 (b) results for brain regions where mean MD values are higher in the AD group.
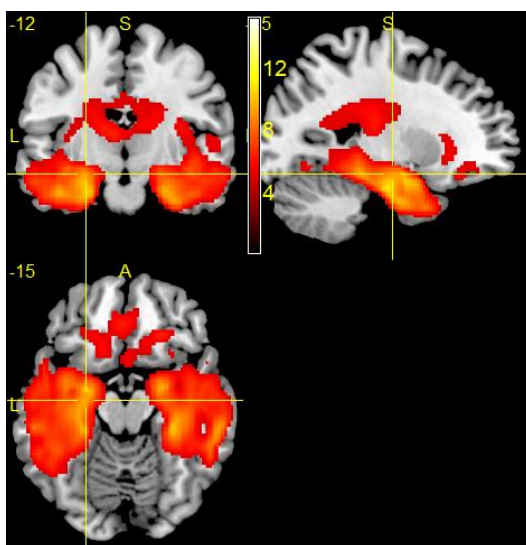

Figure 7.14 (c) results for brain regions where mean L1 values are higher in the AD group.

Figure 7.14 (d) results for brain regions where mean RD values are higher in the AD group.

Figure 7.14 Results for comparing the CN and the AD groups with unpaired two-sample t-tests. Figures (a) - (d) show results for the FA, MD, L1 and RD metrics when no covariates were taken into consideration during the GLM modelling. All images are shown at p < 0.05 corrected for multiple comparisons. The crosshair on image (a) is highlighting the corpus callosum. On image (b), (c) and (d) the crosshairs can be seen pointing to the left temporal lobes.

Results for MD, RD, and L1 highlighted regions of the temporal lobes as the most significantly differing brain regions. Further regions for MD, RD, and L1 included the corpus callosum and the corona radiata.

Figures 7.17(a) and 7.17(b) show the results of the application of contrast vectors opposite to what was used before. Figure 7.17(a) is a good example of how in the case of MD the contrast vector defined in the opposite direction does not yield any significant results. Interestingly this was not the case in figure

Figure 7.17 (a) results for brain regions where mean MD values are higher in the CN group.

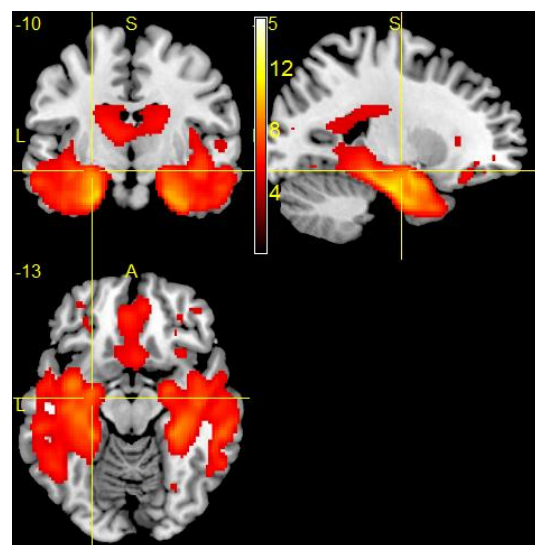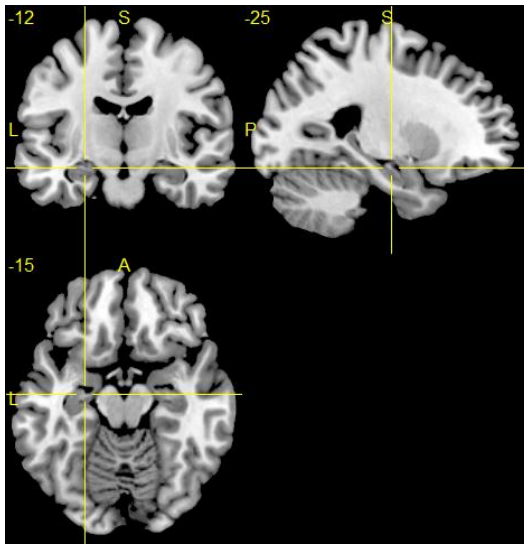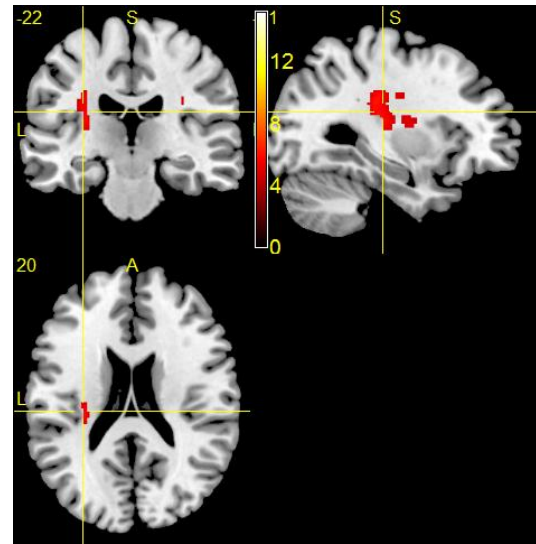**Figure 7.17 (b) results for brain regions where mean FA values are higher in the AD group.**

Figure 7.17 Results for the MD and FA metric can be seen with the application of contrasts in the opposite direction. Both figures are shown at p < 0.05 corrected for multiple comparisons.

7.17(b) where the opposite contrast vector did in fact show significant result even when the p value was corrected for multiple comparisons. One possible explanation could be that there is a countering effect to the degradation of structure in the brain during the progression of Alzheimer's disease. It is possible that this result for FA arose merely from inadequacies in the normalization process and can in fact be considered as a type I error where the null hypothesis was falsely rejected. Either way further research is required to clarify the effects behind this unexpected result.

As mentioned earlier in the introduction to this chapter covariates were used to improve the GLM modelling. Results for MD when all covariates including subject's age, handedness, gender and the derived volumetric ratio were added to the design matrix can be seen in figures 7.20 (a) - 7.20 (b). Modelling was also completed with ANCOVA which allowed for smaller mean differences to become statistically significant as compared to when it wasn't used for the t-tests. Evidence of this added sensitivity caused by the ANCOVA can clearly be seen on the right temporal lobe in figure 7.20 (c).

A similar analysis of FA with the t-test can be seen on figures 7.23(a) and 7.23 (b). Here, significant results could only be found for a less conservative p-value of $p < 0.001$ (without the correction of multiple comparisons problem).
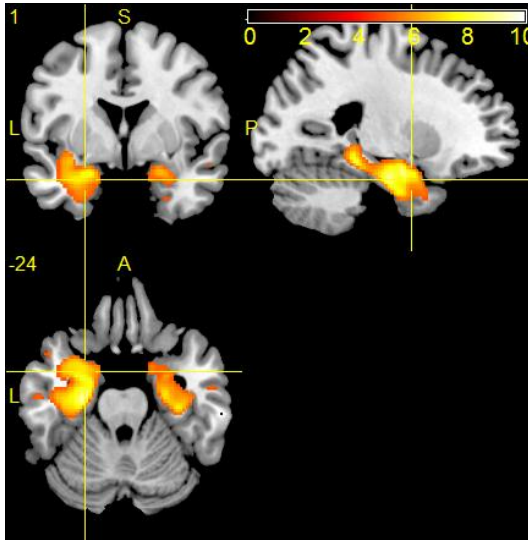
Figure 7.20 (a) results for brain regions where mean MD values are higher in the AD group.
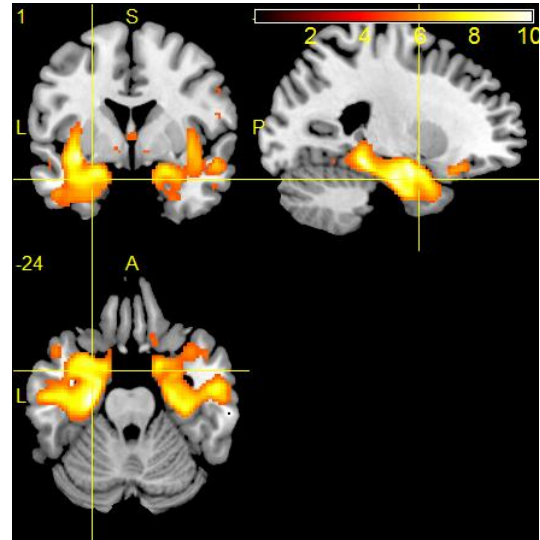
Figure 7.20 (b) results for brain regions where mean MD values are higher in the AD group.

Figure 7.20 Results for MD metric with the modelling including all the covariates are shown in figures (a) and (b). Figures (a) and (b) are shown at p < 0.05 corrected for multiple comparisons. Added sensitivity to mean differences was applied in case of figure (b) with the inclusion of ANCOVA to the GLM modelling
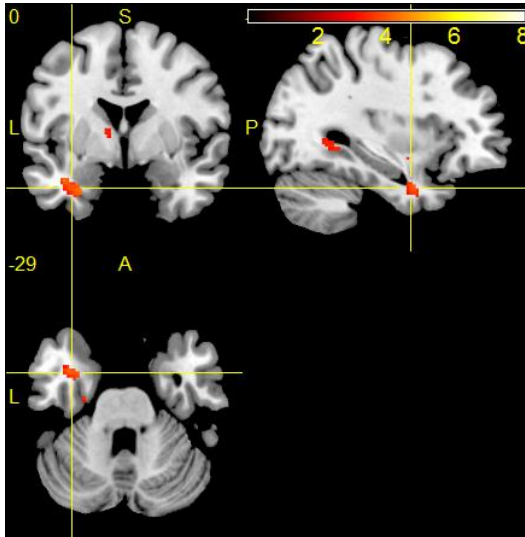
Figure 7.23 (a) results for brain regions where mean FA values are higher in the CN group.
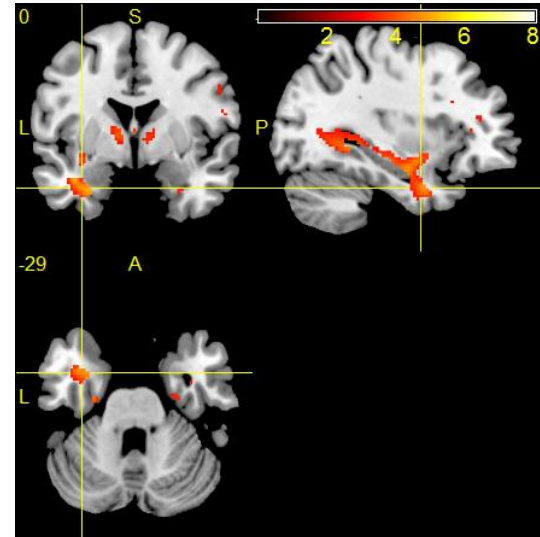
Figure 7.23 (b) results for brain regions where mean FA values are higher in the CN group.

Figure 7.23 a) Results of FA-comparison with all the covariates included   p<0.001. b) Increased sensitivity to mean differences was achieved with ANCOVA in the GLM analysis.

Results for RD and L1 are not included here because both metrics showed correlation with the MD metric both in highlighted areas (seen figure 8.14) and mean values of the metrics. The linear relationship for the values of MD and RD can be seen in Figure 7.24.
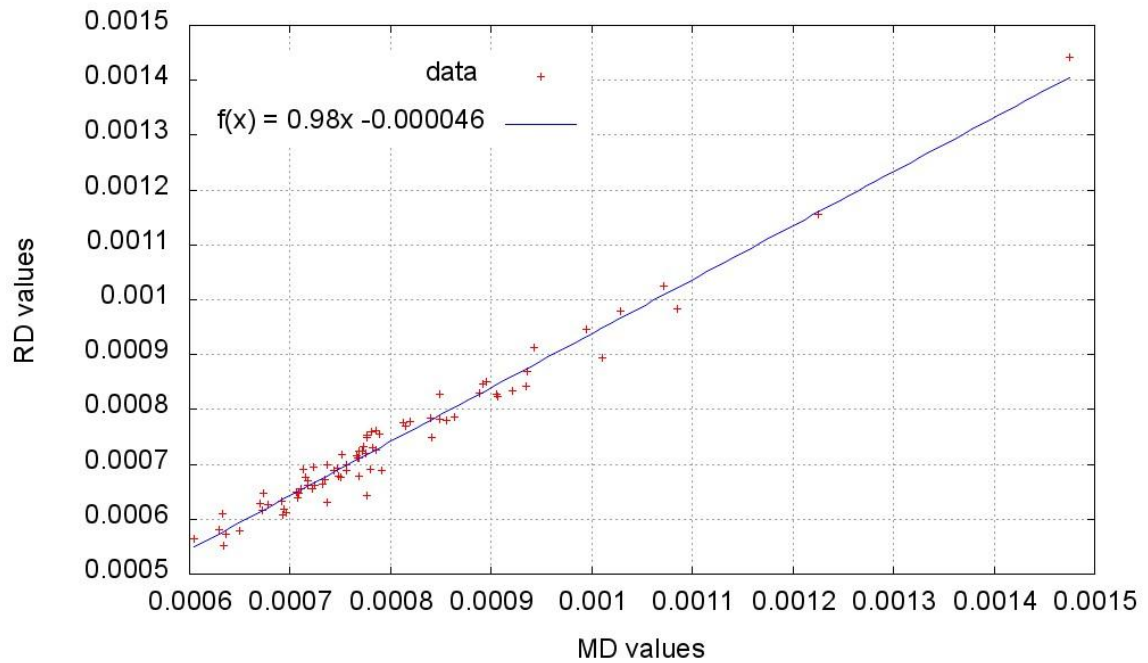
Figure 7.24 Plot showing the linear relationship of MD and RD metrics. The slope of the fitted regression is representative of an almost perfect linear correlation coefficient of +1.

7.4   Region-of-interest (ROI)-level correlation analysis

Another statistical analysis I performed on all of my sample was the evaluation of correlations between the average MD and FA values in all white matter areas (so called ROIs), and the scores of psychological assessments of the MMSE and the RAVLT. For some of my sample I also analysed correlations between ROIs and averaged baseline scores of fludeoxyglucose (FDG) uptake rates during PET scans. The averaged uptake rates were calculated from values of uptake rates in the angular, temporal, and posterior cingulate regions of the brain. In the case of the PET scores only the relevant white matter regions were correlated.

Correlation or the so called Pearson's correlation is the measure of linear correlation between two variables. The correlation ρ is defined as the covariance divided by each of the standard deviations:

$$\rho = \frac{Cov(X,Y)}{\sigma_X \sigma_Y} = \frac{E[\,(X - E[X])([Y - E[Y])]}{\sqrt{(X - E[X])^2}\sqrt{(Y - E[Y])^2}} \tag{7.7}$$
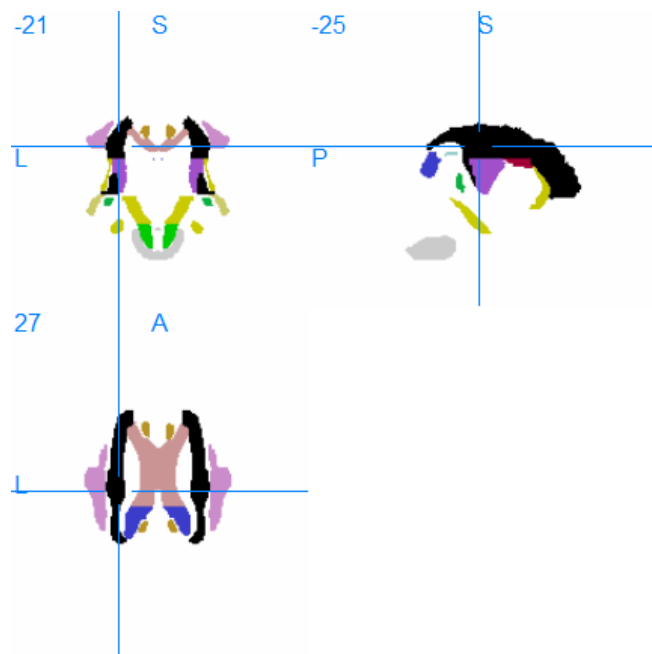
Figure 7.25. The JHU 1mm white matter tractography atlas is shown in the figure. The crosshair can be seen locked in on the left superior corona radiate which among other ROIs significant results resulted for the ROI- level analysis.

A perfect linear correlation is indicated by the coefficient value of +1 and a perfect anti-correlation by -1. Calculations of Pearson's correlation coefficient were performed with the Matlab's *corr()* function. The white matter ROIs were determined with the help of John Hopkins University's (JHU) 1mm white matter tractography atlas [13]. This could be done as both the normalized DTI metrics and the JHU brain atlas were in MNI space.

The white matter regions are summarized in tables 8.1-8.3. Each of the tables contains results for each ROI's correlation coefficient and its corresponding p value. The correlation coefficient describes the direction of linear relationship of the average values of the metrics in the ROIs and the MMSE, RAVLT and PET scores. As expected the results show a positive correlation between MMSE and RAVLT assessment scores and the average FA values in ROIs. And at the same time there is a negative correlation between average MD values and these assessments.

Significant positive linear correlation was also seen between average values of FA and MD for the PET scores summarized in table 8.3. Pet scores showed the same linear relationship for the FA and MD metric as in the case of the psychological assessments.

Results of the correlation analyses for a significance level of $\alpha = 0.001$ are showed in tables 8.1-8.3. Statistically significant correlations were mostly observed in the case of MD. The significant correlation of MD provided further validation of the results of the whole brain voxel-wise analyses in chapters 7.2 and 7.3.

white matter regions	MMSE			
	FA		MD	
	correlation	p value	correlation	p value
Genu of corpus callosum			-0.2916	P<< 0.001
Body of corpus callosum			-0.2704	P<< 0.001
Splenium of corpus callosum			-0.2995	P<< 0.001
Fornix (column and body of fornix)	0.3214	P<< 0.001	-0.2497	0.0002
Cerebral peduncle L			-0.2903	P<< 0.001
Cerebral peduncle R			-0.2303	0.0007
Retrolenticular part of internal capsule L			-0.3014	P<< 0.001
Retrolenticular part of internal capsule R			-0.2529	0.0002
Anterior corona radiata L	0.2331	0.0006	-0.2927	P<< 0.001
Anterior corona radiata R			-0.2898	P<< 0.001
Superior corona radiata L			-0.2604	0.0001
Superior corona radiata R			-0.2504	0.0002
Posterior corona radiata L			-0.3076	P<< 0.001
Posterior corona radiata R			-0.2487	0.0002
Posterior thalamic radiation L	0.2412	0.0004	-0.3239	P<< 0.001
Posterior thalamic radiation R			-0.2996	P<< 0.001
Sagittal stratum L			-0.4159	P<< 0.001
Sagittal stratum R			-0.3905	P<< 0.001
Cingulum (cingulate gyrus) L			-0.3155	P<< 0.001
Cingulum (cingulate gyrus) R			-0.3115	P<< 0.001
Cingulum (hippocampus) L	0.3321	P<< 0.001	-0.4524	P<< 0.001
Cingulum (hippocampus) R			-0.3191	P<< 0.001
Fornix (cres) Stria terminalis L	0.3450	P<< 0.001	-0.4668	P<< 0.001
Fornix (cres) Stria terminalis R	0.3480	P<< 0.001	-0.4493	P<< 0.001
Superior longitudinal fasciculus L	0.2454	0.0003	-0.3766	P<< 0.001
Superior longitudinal fasciculus R			-0.2791	P<< 0.001
Superior fronto-occipital fasciculus L			-0.2571	0.0001
Tapetum L	0.2371	0.0005		

Table 7.1 Results for baseline MMSE scores are shown in the cases of the FA and MD

white matter regions	RAVLT			
	FA		MD	
	correlation	p value	correlation	p value
Body of corpus callosum			-0.2609	P<< 0.001
Splenium of corpus callosum			-0.2896	P<< 0.001
Fornix (column and body of fornix)	0.3415	P<< 0.001	-0.3072	P<< 0.001
Cerebral peduncle L			-0.2401	P<< 0.001
Retrolenticular part of internal capsule L			-0.2834	P<< 0.001
Retrolenticular part of internal capsule R			-0.2282	0.0008
Anterior corona radiata L			-0.2525	0.0002
Anterior corona radiata R			-0.2553	0.0001
Superior corona radiata L			-0.2379	0.0004
Posterior corona radiata L			-0.2438	0.0003
Posterior corona radiata R			-0.2297	0.0007
Posterior thalamic radiation L	0.2279	0.0008	-0.3246	P<< 0.001
Posterior thalamic radiation R			-0.2749	P<< 0.001
Sagittal stratum L	0.2265	0.0009	-0.3890	P<< 0.001
Sagittal stratum R			-0.3074	P<< 0.001
Cingulum (cingulate gyrus) L	0.2319	0.0006	-0.2660	P<< 0.001
Cingulum (cingulate gyrus) R			-0.2955	0,00001
Cingulum (hippocampus) L	0.3132	P<< 0.001	-0.4369	P<< 0.001
Cingulum (hippocampus) R			-0.3160	P<< 0.001
Fornix (cres) Stria terminalis L	0.3468	P<< 0.001	-0.4797	P<< 0.001
Fornix (cres) Stria terminalis R	0.3763	P<< 0.001	-0.4224	P<< 0.001
Superior longitudinal fasciculus L	0.2423	0.0004	-0.3612	P<< 0.001
Superior longitudinal fasciculus R			-0.2666	0.00008

Table 7.2 Results for baseline RAVLT scores are shown in the cases of the FA and MD

white matter regions	PET			
	FA		MD	
	correlation	p value	correlation	p value
Genu of corpus callosum	0.2662	P<< 0.001	-0.3814	P<< 0.001
Body of corpus callosum	0.3269	P<< 0.001	-0.4063	P<< 0.001
Splenium of corpus callosum	0.2803	P<< 0.001	-0.4170	P<< 0.001
Fornix (column and body of fornix)	0.3383	P<< 0.001	-0.3089	P<< 0.001
Retrolenticular part of internal capsule L			-0.3090	P<< 0.001
Retrolenticular part of internal capsule R			-0.2655	P<< 0.001
Anterior corona radiata L			-0.2745	P<< 0.001
Anterior corona radiata R			-0.2839	P<< 0.001
Superior corona radiata L			-0.2971	P<< 0.001
Superior corona radiata R			-0.3456	P<< 0.001
Posterior corona radiata L			-0.2956	P<< 0.001
Posterior corona radiata R			-0.3190	P<< 0.001
Posterior thalamic radiation L			-0.2885	P<< 0.001
Posterior thalamic R			-0.3303	P<< 0.001
Sagittal stratum L			-0.401	P<< 0.001
Sagittal stratum R			-0.4270	P<< 0.001
Cingulum (cingulate gyrus) L	0.2889	0.00002	-0.332	P<< 0.001
Cingulum (cingulate gyrus) R	0.2853	0.00003	-0.4146	P<< 0.001
Cingulum (hippocampus) L			-0.2871	P<< 0.001
Cingulum (hippocampus) R			-0.3209	P<< 0.001
Fornix (cres) Stria terminalis L	0.3340	P<< 0.001	-0.3934	P<< 0.001
Fornix (cres) Stria terminalis R	0.3933	P<< 0.001	-0.4517	P<< 0.001
Superior longitudinal fasciculus L	0.2854	P<< 0.001	-0.3827	P<< 0.001
Superior longitudinal fasciculus R	0.3275	P<< 0.001	-0.4117	P<< 0.001
Superior fronto-occipital fasciculus L			-0.3532	P<< 0.001
Superior fronto-occipital fasciculus R			-0.3017	P<< 0.001
Uncinate fasciculus L			-0.2388	0.0004
Tapetum R	0.245996	0.000309	-0.2652	0.00009

Table 7.3 Results for baseline PET scores are shown in the cases of the FA and MD

8   Conclusions and summary

Summarizing results I can say that I was able to show statistically significant differences between the structure of white matter in groups CN, MCI and AD. Results in the change of white matter structure were most prominently visible between CN and AD groups, in regions of the temporal lobes, corpus callosum, corona radiata, and cingulum. Thus I was able to validate previous findings of structural changes identified using different methods different from mine. [5,6,29]

All results put forward in my thesis were inferred from raw data collected from the ADNI database. The raw data had undergone pre-processing steps followed by spatial normalization. The pre-processing steps included the correction of EPI- and eddy-current-related distortions. The normalization procedure involved steps of co-registration of DTI images to T1w images, the segmentation of T1w images, the spatial normalization of DTI-parameter images into MNI space and the smoothing of normalized DTI images. Statistical analyses were conducted on spatially normalized DTI-parameter images to determine structural changes in white matter between CN, MCI and AD groups. General evaluation of changes were shown using ANOVA. T-tests were used in order to determine specific changes between groups. Specific covariates were also incorporated into the analyses conducted with t-tests to increase the statistical power of results.

The concordance of my results to the literature underlined the importance of VBA as a possible substitute of TBSS based methods. One can argue that the co-registration quality is far more superior in case of TBSS, however this better registration is achieved at a cost of severe data reduction. As my VBA shows microstructural changes are not limited to the vicinity of highest FA values, but quite the opposite they can extend to the whole extent of the white matter in affected regions.

Higher mean FA values for the AD group were found in the region of the corona radiate during the comparison of CN and AD groups. Explanations for this unexpected finding could possibly involve either false positives occurring as a result of inadequate normalization methods or could equally possibly point towards the discovery of a compensatory effect for the structural disintegration of white matter in the progression

of Alzheimer's disease. Further research will be required before to investigate if these changes could signify reparatory mechanisms.

The ROI-based correlation analyses shows the importance of multi parametric analyses, i.e. the observed correlations for the FA metric seem to be spatially more specific, however, the correlations for the MD metric underline that microstructural changes in AD and MCI are not limited to the medial temporal lobes and the hippocampi, but affect the whole brain even in early stages of the disease.

In conclusion it can be said that promising steps have been made towards the development of a new processing pipeline for the identification of white matter microstructural changes using DTI. These changes could potentially serve as a biomarker in more complex evaluation methods in the future for definitive diagnosis of mild cognitive impairment as a precursory state and monitoring the progression of definite Alzheimer's disease in affected patients.

9   Acknowledgements

I would like to thank my supervisor, Dr. Lajos R. Kozák for letting me join his research group at the MR Research Centre of Semmelweis University for the duration of my thesis.

I would also like to thank Gyula Gyebnár, a PhD student of Dr. Kozák for his invaluable support throughout the writing of my thesis. His knowledge of statistics and DTI preprocessing methods greatly helped my work.

I would also like to thank Dr. Dávid Légrády, my internal supervisor at the Department of Nuclear Techniques for his help and support throughout my master's degree.

Last but not least I would like to thank the director of the MR Research Centre, professor Gábor Rudas for granting me access to the centre's resources.

10 Literature

[1]   Derek K. Jones: *„Diffusion MRI: Theory, methods, and applications"* , Oxford University press (2011).

[2]   *"Human brain function";* Edited by*:* Richard S.J. Frackowiak, Karl J. Friston, Christopher D. Frith, Raymond J. Dolan, Cathy J. Price, Semir Zeki, John T. Ashburner and William D. Penny

[3]   A. Burns, S. Iliffe : *"Alzheimer's disease",* BMJ; 2009

[4]   Bach et al.: "*Methodological considerations on tract-based spatial statistics*", NeuroImage Volume 100; 2014

[5]   J Acosta-Cabronero: *"Diffusion tensor imaging in Alzheimer's disease: insights into the limbic-diencephalic network and methodological considerations"*, Frontiers in Aging Neuroscience;2014

[6]   Sexton et al.: "*A meta-analysis of diffusion tensor imaging in mild cognitive impairment and Alzheimer's disease."* , Neurobiology of aging; 2011

[7]   Filippi M, Agosta F: *"Structural and Functional Network Connectivity Breakdown in Alzheimer's Disease Studied with Magnetic Resonance Imaging Techniques"* , *Journal of Alzheimer's Disease, vol. 24;2011*

[8]   Petersen et al.: *"Alzheimer's Disease Neuroimaging Initiative (ADNI) ",Neurology. 2010.*

[9]   Schwarz et al.: *"Improved DTI registration allows voxel-based analysis that outperforms tract-based spatial statistics.*" , NeuroImage, 2014

[10]   Einstein A.: *"Investigations on the theory of Brownian Motion";*1956*.*

[11]   Neuroimaging Informatics Technology Initiative: *http://nifti.nimh.nih.gov/*

[12]   EPI correction: *http://sites.cardiff.ac.uk/cubric/cubric-users/user-documentation/mri-resources/mri-how-to/effective-epi-distortion-correction-in-exploredti-v4-8-3/*

[13]   MNI space: http://www.nil.wustl.edu/labs/kevin/man/answers/mnispace.html

[14]   JHU atlas: http://www.ncbi.nlm.nih.gov/pubmed/18255316

[15]   SPM12 manual: *http://www.fil.ion.ucl.ac.uk/spm/doc/manual.pdf*

[16]   Dr. Lajos R. Kozák.: *Diffusion tensor imaging [Lecture notes]*

[17]   P Winston.*: The physical and biological basis of quantitative parameters derived from diffusion MRI*; 2002;

[18]   J. Jellison et al.: *"Diffusion Tensor Imaging of Cerebral White Matter: A Pictorial Review of Physics, Fiber Tract Anatomy, and Tumor Imaging Patterns"*, AJNR; 2004

[19]   Le Bihan et al. (2006), "*Artifacts and Pitfalls in Diffusion MRI*", Journal of magnetic resonance imaging; 2006

[20]   *http://dbm.neuro.uni-jena.de/imas/intensity-gauss.jpg*

[21]   *http://dbm.neuro.uni-jena.de/imas/Bayes-apriori.jpg*

[22]   P. J. Basser, C. Pierpaoli : *"Microstructural and physiological features of tissues elucidated by quantitative-diffusion-tensor MRI"*, Journal of magnetic resonance; 1996

[23]   Mudher A, Lovestone S.: *"Alzheimer's disease-do tauists and baptists finally shake hands?"* Trends in Neurosciences;2002

[24]   T N Tombaugh, N J McIntyre: "*The mini-mental Status Examination: A comprehensive Review*". JAGS, 1992

[25]   T. Barzotti et al.: *"Correlation between cognitive impairment and the Rey auditory-verbal learning test in a population with Alzheimer disease."* Archives of Gerontology and Geriatrics;2004

[26]   ExploreDTI: *http://www.exploredti.com/generalinfo.htm*

[27]   Bonferroni, C. E., „*Teoria statistica delle classi e calcolo delle probabilità*", Pubblicazioni del R Istituto Superiore di Scienze Economiche e Commerciali di Firenze; 1936

[28]   Amlien IK, Fjell AM.: *"Diffusion tensor imaging of white matter degeneration in Alzheimer's disease and mild cognitive impairment."*; Neuroscience, Volume 276; 2014

[29]   T. M. Nir et al.: *"Effectiveness of regional DTI measures in distinguishing Alzheimer's disease, MCI, and normal aging"*, NeuroImage: Clinical;2013